Speed Ripple Minimization in PM Synchronous Motor Using Iterative Learning Control

Weizhe Qian, S. K. Panda, *Senior Member, IEEE*, and J. X. Xu, *Senior Member, IEEE*

***Abstract*—Permanent-magnet synchronous motor (PMSM) drives are widely used for high-performance industrial servo applications where torque smoothness is an essential requirement. However, one disadvantage of PMSM is parasitic torque pulsations, which induce speed oscillation that deteriorates the drive performance particularly at low-speeds. To suppress these speed ripples, two iterative learning control (ILC) schemes implemented in time domain and frequency domain respectively are proposed in this paper. Although a conventional proportional-integral (PI) speed controller does suppress speed ripples to a certain extent, it is not adequate for many high performance applications. Thus, the proposed plug-in ILC controller is applied in conjunction with a PI speed controller to further reduce the periodic speed ripples. Experimental verification of the two schemes is carried out, and test results obtained demonstrate that the scheme implemented in frequency domain has better performance in reducing speed ripples than that implemented in time domain because of the elimination of forgetting factor that is indispensable for robustness in time domain learning method.**

***Index Terms*—Learning control systems, motor drives, motor speed control, permanent-magnet (PM) motors, synchronous motors.**

I. Introduction

PERMANENT-MAGNET (PM) synchronous motor drives are widely used in robotics, machine tools, and other high-performance industrial servo applications. Permanent-magnet synchronous motors (PMSMs) are preferred over the traditional brush-type dc motors because of the absence of mechanical commutators, which reduces mechanical wear and tear of the brushes and increases the life span of the motor. As compared to induction motors, PMSMs are still favored for high-performance servo applications because of their high efficiency, power density and torque-to-inertia ratio, which make them a suitable choice for variable-speed direct-drive applications.

However, the main disadvantage of PMSMs is the parasitic torque pulsations [1]. Presence of these torque pulsations results in instantaneous torque that pulsates periodically with rotor position. These pulsations are reflected as periodic oscillations in the motor speed, especially for low-speed operation. At higher operating speeds, these torque pulsations are naturally filtered off by the rotor and load inertias and therefore, are not reflected back in the motor speed. But in the absence of mechanical gears in direct-drive servos, the motor drive has to operate at low-speeds. These speed oscillations severely limit the performance of the servo especially in high-precision tracking applications. Moreover, the oscillations produce undesirable mechanical vibration on the load side.

There are various sources of torque pulsations in a PMSM such as the cogging, flux harmonics, errors in current measurements, and phase unbalancing. In view of the increasing popularity of PMSMs in industrial applications, the suppression of pulsating torques has received much attention in recent years. Broadly speaking, these techniques can be divided into two groups: one focusing on the improvement of motor design and the other emphasizing on using active control of stator current excitations [1]. From the motor design viewpoint, skewing the stator lamination stacks or rotor magnets, arranging proper winding distribution, and other motor design features reduce cogging torque to a certain degree but do not completely eliminate it [2]. Moreover, special machine design techniques additionally increase the complexity in the production process, which results in higher machine cost.

The second approach, which is of our interest, concentrates on using an additional control effort to compensate these periodic torque pulsations. One of the earliest methods proposed in [3] and [4] is to use pre-programmed stator current excitation to cancel torque harmonic components. However, in such a method, sufficiently accurate information of the PMSM parameters, in particular the characteristics of torque ripples are required, and a small error or variations in parameters can lead to an even higher torque ripple due to the open-loop feed-forward control. In view of the inherent limitations of these open-loop control schemes, alternative approaches applying closed-loop control algorithms with online estimation techniques (e.g., a self-commissioning scheme [5] and an adaptive control algorithm [6]) to achieve torque pulsation minimization have been proposed. These real-time control schemes are implemented either in speed or in current (torque) loops. In torque control schemes, one popular way is to regulate torque by using online estimated torque based on electrical subsystem variables (currents and voltages) only. Various algorithms have been proposed for instantaneous torque estimation [7]–[10]. On the other hand, this approach can be used only for those torque ripple components that are observable from an electrical subsystem—ripples due to mechanical part (e.g., cogging torque and load oscillations) cannot reflect in electrical subsystem variables, and hence uncontrollable [6]. An alternative technique is to use a torque transducer with high bandwidth output to measure the real-time torque signal, which can then be applied as the feedback information. This, however, increases the cost of drive system. While all of the techniques described above seek to attenuate torque

Manuscript received July 1, 2003. Paper no. TEC-00079-2003.

The authors are with the Department of Electrical and Computer Engineering, National University of Singapore, Singapore 117576 (e-mail: eleskp@nus.edu.sg).

Digital Object Identifier 10.1109/TEC.2004.841513

pulsations by adjusting the stator current excitations, an alternative approach relies on a closed-loop speed regulator to accomplish the same objective indirectly, i.e., the attenuation of torque ripples [6], [8]. All possible sources of torque ripples are observable from rotor speed, hence this method has potential for complete torque ripples minimization. However, the quality of speed feedback and slow dynamics of the outer speed loop limit the dynamic performance of the algorithm.

In this paper, two iterative learning control schemes implemented in the time domain as well as in the frequency domain, respectively, have been proposed with the objective of minimizing periodic speed ripples originated by torque pulsations. Regardless of the difference between their control structures, both control schemes have the same drive configuration. The proposed iterative learning control (ILC) controller is applied in conjunction with the conventional proportional-integral (PI) speed controller, which provides the main reference current. During steady state, the proposed controller generates the compensation current that together with the main reference current is utilized to minimize the speed ripples. Conventional PI current controllers are used in the inner control loops to generate the control voltages to shape pulsewidth-modulated (PWM) signals. The performances of both ILC control schemes have been evaluated through extensive experimental investigations. Test results obtained demonstrate improvements in the steady-state speed response and therefore validate the effectiveness of both ILC schemes. A comparison between the two schemes also shows the advantage of the scheme implemented in frequency domain, because of the elimination of the forgetting factor used for robustness in the time-domain learning method, which further enhances the effectiveness in suppressing speed ripples.

The remainder of this paper is organized as follows. In Section II, the mathematical model of the PMSM is given. Section III briefly describes the sources of torque pulsations and the resultant speed ripples in PMSM drive. In Section IV, the proposed ILC schemes are explained, and PMSM drive setup used in experiments is introduced in Section V. Section VI presents and discusses the experimental results. Finally, some concluding remarks are made in Section VII.

II. PMSM Model

With assumptions that the PMSM is unsaturated and eddy currents and hysteresis losses are negligible, the stator d, q-axes voltage equations of the PMSM in the synchronous rotating reference frame are given by

$$\frac{di_{ds}}{dt} = -\frac{R}{L_d} i_{ds} + \frac{L_q}{L_d}\omega_e i_{qs} + \frac{1}{L_d} v_{ds} \tag{1}$$

$$\frac{di_{qs}}{dt} = -\frac{R}{L_q} i_{qs} - \frac{L_d}{L_q}\omega_e i_{ds} - \frac{\omega_e}{L_q}\psi_{dm} + \frac{1}{L_q} v_{qs} \tag{2}$$

where i_{ds} and i_{qs} are the d, q-axes stator currents, v_{ds} and v_{qs} are the d, q-axes voltages, L_d and L_q are the d, q-axes inductances, while R and ω_e are the stator resistance and electrical angular velocity, respectively [11]. The flux linkage ψ_{dm} is due to rotor magnets linking the stator. It has been further assumed that as the surface mounted PMSM is nonsalient, L_d and L_q are equal and are taken as L.

Using the method of field-oriented control of the PMSM, the d-axis current is controlled to be zero to maximize the output torque. The motor torque is given by

$$T_m = \frac{3}{2}\frac{P}{2}\psi_{dm} i_{qs} = k_t i_{qs} \tag{3}$$

in which $k_t (=(3/2XP/2)\psi_{dm})$ is the torque constant and P is the number of poles in the motor.

The equation of the motor dynamics is

$$\frac{d\omega_m}{dt} = -\frac{B}{J}\omega_m + \frac{k_t}{J} i_{qs} - \frac{T_l}{J} \tag{4}$$

where ω_m is the mechanical rotor speed, T_l is the load torque, B is the frictional coefficient and J is the total inertia (motor and load).

III. Analysis of Torque Pulsations

A. Flux Harmonics

Due to the nonsinusoidal flux density distribution in the airgap, the resultant flux linkage between the permanent magnet and the stator currents contains harmonics of the order of $5, 7, 11, \ldots$ in the a-b-c frame (triple harmonics are absent in Y-connected stator windings) [9]. In the synchronous rotating reference frame, the corresponding harmonics appear as the 6th and the multiples of 6th-order harmonic components, and can be expressed as

$$\psi_{dm} = \psi_{d0} + \psi_{d6}\cos 6\theta_e + \psi_{d12}\cos 12\theta_e + \cdots \tag{5}$$

where ψ_{d0}, ψ_{d6}, and ψ_{d12} are the dc, 6th, and 12th harmonic terms of the d-axis flux linkage, respectively, while θ_e is the electrical angle. Combining (3) and (5), we get

$$\begin{aligned} T_m &= T_0 + T_6\cos 6\theta_e + T_{12}\cos 12\theta_e + \cdots \\ &= T_0 + \Delta T_{m,6} + \Delta T_{m,12} + \cdots \end{aligned} \tag{6}$$

where T_0, T_6, and T_{12} are the dc component, 6th, and 12th harmonic torque amplitudes respectively. Equation (6) indicates that the 6th and 12th torque harmonics produced mainly due to nonsinusoidal flux distribution are periodic in nature.

B. Current Offset Error

The dc offset in stator current measurements also leads to pulsating torque [12]. Stator currents are measured and transduced into voltage signals by current sensors and then transformed into digital form by analog-to-digital (A/D) converters. The presence of any unbalanced dc supply voltage in the current sensors and inherent offsets in the analog electronic devices give rise to dc offsets. Letting the dc offsets in the measured currents of phases a and b be Δi_{as} and Δi_{bs}, respectively, the "measured" q-axis current i_{qs}-AD can be expressed as

$$i_{qs-AD} = i_{qs} + \Delta i_{qs} \tag{7}$$

where

$$\Delta i_{qs} = \frac{2}{\sqrt{3}} \cos(\theta_e + \alpha) \sqrt{\Delta i_{as}^2 + \Delta i_{as} \Delta i_{bs} + \Delta i_{bs}^2} \quad (8)$$

and α is a constant angular displacement and is dependent on Δi_{as} and Δi_{bs}. As $\theta_e = 2\pi f_s t$, it is shown that Δi_{qs} oscillates at the fundamental electrical frequency. Assuming the measured currents exactly follow the reference currents, the actual motor current is given by

$$i_{qs} = i_{qs-AD} - \Delta i_{qs} = i_{qs}^* - \Delta i_{qs}. \quad (9)$$

Using (3) and (9), we get

$$T_m = k_t (i_{qs}^* - \Delta i_{qs}) = T_m^* - \Delta T_{m,1}. \quad (10)$$

Substituting (8) into (10), $\Delta T_{m,1}$ can be obtained as

$$\Delta T_{m,1} = k_t \frac{2}{\sqrt{3}} \cos(\theta_e + \alpha) \sqrt{\Delta i_{as}^2 + \Delta i_{as} \Delta i_{bs} + \Delta i_{bs}^2}. \quad (11)$$

Equation (11) shows that the offsets in current measurement give rise to a torque oscillation at the fundamental frequency f_s.

C. Current Scaling Error

The output of the current sensor must be scaled to match the input of the A/D converter, and in the digital form, the controller re-scales the value of the A/D output to obtain the actual value of the current. As such, scaling errors of the currents are inevitable [12]. Again assuming ideal current tracking, the measured phase currents are

$$i_{as-AD} = i_{as}^* = I \cos \theta_e \quad (12)$$

$$i_{bs-AD} = i_{bs}^* = I \cos\left(\theta_e - \frac{2\pi}{3}\right). \quad (13)$$

Denoting the scaling factors of the phases a and b currents as K_a and K_b, respectively, the phase currents as seen from the controller are

$$i_{as} = I \cos \theta_e / K_a \quad (14)$$

$$i_{bs} = I \cos\left(\theta_e - \frac{2\pi}{3}\right) \Big/ K_b. \quad (15)$$

From similar analysis as in the current offset error, Δi_{qs} can be evaluated as

$$\begin{aligned} \Delta i_{qs} &= i_{qs-AD} - i_{qs} \\ &= \left(\frac{K_a - K_b}{K_a K_b}\right) \frac{I}{\sqrt{3}} \left[\cos\left(2\theta_e + \frac{\pi}{3}\right) + \frac{1}{2}\right]. \end{aligned} \quad (16)$$

From (10) and (16), the torque error is

$$\Delta T_{m,2} = \left(\frac{K_a - K_b}{K_a K_b}\right) \frac{k_t I}{\sqrt{3}} \left[\cos(2\theta_e + \frac{\pi}{3}) + \frac{1}{2}\right]. \quad (17)$$

Equation (17) shows that the scaling error causes the torque to oscillate at twice the fundamental frequency $2f_s$.

These analyses indicate that the electromagnetic torque consists of a dc component together with the 1st, 2nd, 6th, and 12th harmonic components. The control objective is to suppress these periodic torque ripples by the proposed ILC schemes indirectly.

D. Speed Ripples Caused by Torque Pulsations

The plant transfer function between the motor speed and the torque is

$$\omega_m(s) = \frac{T_m(s) - T_l(s)}{Js + B} \quad (18)$$

where $T_m = f(\psi_{dm}, i_{qs}, \omega_m)$. It can be seen that the speed would oscillate at the same harmonic frequencies as those of ΔT_m, especially at low operating speeds. It is imperative that to minimize the speed ripples the sources of these speed oscillations—torque pulsations need to be minimized. However, for suppression of torque ripples it is necessary to measure or estimate the instantaneous torque, which makes the drive system expensive (by using torque transducer) or complicated (by using torque observer). Therefore, in the proposed scheme as described in the next section, speed information which is already available for the closed-loop speed control purpose, is utilized to compensate for torque ripples indirectly. Consequently, the suppression of torque ripples leads to reduction in speed ripples.

IV. ILC Scheme for PMSM

Iterative learning control is an approach to improving the tracking performance of systems that operate repetitively over a fixed time interval. It is useful for problems in which a system must be able to follow different types of inputs, in the face of design, modeling uncertainty or system nonlinearities in response to periodic disturbances in inputs. ILC is actually an error correction algorithm and a memory that stores the previous output data and error information.

A. ILC Controller Implemented in Time Domain

In our scheme, we have adopted a P-type learning controller employing the combined *previous cycle feedback* (PCF) and *current cycle feedback* (CCF) scheme. The P-type algorithm is simple to implement, unlike in the D-type since differentiation of the speed signal is unnecessary, hence noise build-up in input update caused by the differentiation of speed signal can be avoided. In [14], a mathematically rigorous treatment of the robustness and convergence of the P-type learning control algorithm is given. It is found that the introduction of a forgetting factor α increases the robustness of the P-type algorithm against noise, initialization error and fluctuation of system dynamics. The proposed ILC scheme in time domain is illustrated in Fig. 1, and the following learning law is used:

$$u_{i+1}(t) = (1 - \alpha) u_i(t) + \Phi e_i(t) + \Gamma e_{i+1}(t) \quad (19)$$

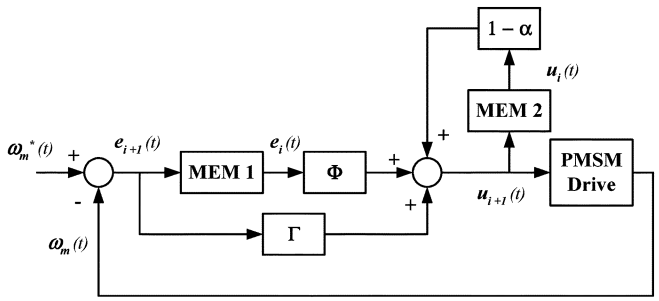

Fig. 1. Block diagram of the ILC scheme implemented in the time domain.

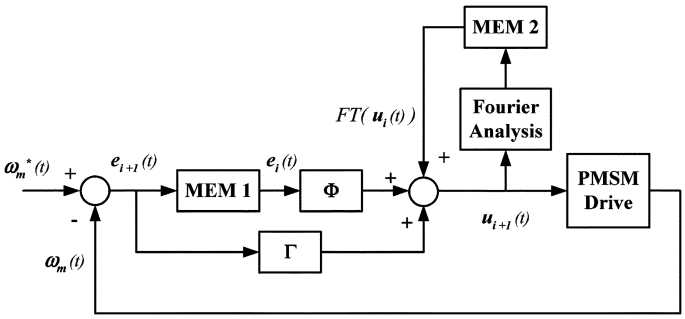

Fig. 2. Block diagram of the ILC scheme implemented in the frequency domain.

where $i = 1, 2, 3, \ldots$ is the iteration number; $u_i(t)$ is the control signal, namely, reference compensation q-axis current generated from ILC; $e_i(t)$ is the speed error signal or $\omega_m^*(t) - \omega_m(t)$; α is the forgetting factor; and Φ and Γ are the PCF and CCF gains, respectively.

To determine the learning gain Φ, assuming perfect tracking of the inner-loop current controller

$$T_m(t) = T_m^*(t) = k_t i_{qs}^*(t) \tag{20}$$

and substituting (20) into (4) yields

$$\frac{d\omega_m(t)}{dt} = -\frac{B}{J} w_m + \frac{k_t}{J} i_{qs}^*(t) - \frac{1}{J} T_l. \tag{21}$$

For the purpose of convergence, the following condition must hold according to [13]:

$$\left\| 1 - \frac{k_t}{J}\Phi \right\| < 1. \tag{22}$$

Denoting $0 < k_t/J \leq |k_t/J|_{\max}$, the inequality in (22) can be solved as

$$0 < \Phi < \frac{2}{|k_t/J|_{\max}}. \tag{23}$$

From the knowledge of the range of d-axis flux linkage ψ_{dm} (since k_t depends on ψ_{dm}) and the total inertia J, the learning gain Φ can be determined. To achieve a faster rate of convergence, the value of Φ should approach $2|k_t/J|_{\max}^{-1}$. However, a conservative choice of Φ that ensures stability and reasonably fast convergence would suffice. Theoretically the CCF gain, Γ does not affect the convergence in the iteration axis of the learning controller [15]. However, having Γ that is too large will cause over-amplification of error or noise signals in the input updating and the corresponding control output will tend to be large, leading to the eventual divergence of the output. As before, a conservative choice of Γ such that $\tau \leq \phi$ would suffice in producing good results.

B. ILC Controller Implemented in the Frequency Domain

Unfortunately, the introduction of the forgetting factor in the time-domain learning scheme only ensures the tracking errors within a certain bound, and further improvement is limited with the consideration of robustness. Under such conditions, we further implement learning control in the frequency domain by means of Fourier series expansion [16] as shown in Fig. 2. Fourier-series-based learning enhances the robustness of iterative learning and in the meantime maintains the possibility of reducing tracking errors to zero theoretically. Note that there always exists system noise or other small nonrepeatable factors in the system. Accumulation of those components contained in $u_i(t)$ may degrade the approximation precision of the controller for each new trial. Fourier-series-based learning mechanism, on the other hand, updates coefficients of the learned frequency components over the entire learning period according to (25), which takes an averaging operation on noise and is able to remove the majority of noise and nonrepeatable factors. Consequently, there is no need to introduce the forgetting factor in this scheme. The repeatability of speed ripples implies that only countable integer multiples of the frequency are involved. This ensures the feasibility of constructing componentwise learning in the frequency domain. Following is the control law:

$$u_{i+1}(t) = FT(u_i(t)) + \Phi e_i(t) + \Gamma e_{i+1}(t) \tag{24}$$

$$FT(u_i(t)) = \psi^T \cdot \frac{2}{T} \int_0^T u_i(t)\psi_1 dt \tag{25}$$

where

$$\psi = [0.5 \quad \cos\omega_e t \quad \cdots \quad \cos N\omega_e t \quad \sin\omega_e t \quad \sin 2\omega_e t \quad \cdots \quad \sin N\omega_e t]^T \tag{26}$$

$$\psi_1 = [1 \quad \cos\omega_e t \quad \cdots \quad \cos N\omega_e t \quad \sin\omega_e t \quad \sin 2\omega_e t \quad \cdots \quad \sin N\omega_e t]^T \tag{27}$$

$$\omega_e = 2\pi f_s = \frac{2\pi}{T}. \tag{28}$$

Parameter ω_e is the fundamental angular frequency of the speed ripples and N can be chosen such that Fourier series expansion covers the Nth-order harmonics of the fundamental frequency.

V. Implementation of Drive System

Fig. 3 shows the overall speed ripple minimization scheme. During the transient state, the ILC is made inactive and i_{qs}^* is provided only by the PI speed controller output, i_{q0}^*. When steady state is reached, the ILC is applied and it provides the additional compensation term Δi_{qs}^* to i_{q0}^* so as to minimize the speed ripples. The performance of the drive system using the ILC scheme is compared with the scheme using only the PI controller. The sampling times for the controllers are: current controller 200 μs and the speed controller 800 μs. The gains

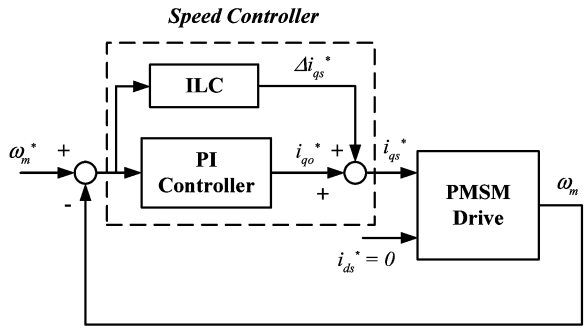

Fig. 3. Block diagram of the speed control loop used in PMSM drive system.

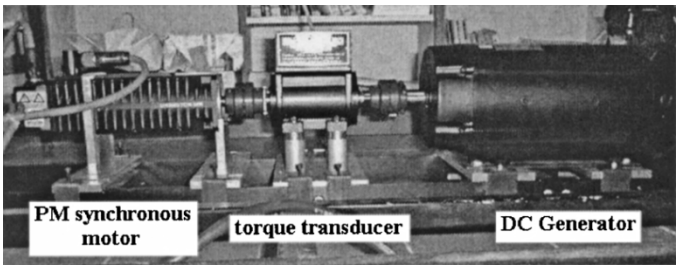

Fig. 4. Photograph of the PMSM and the dc generator used in experiments.

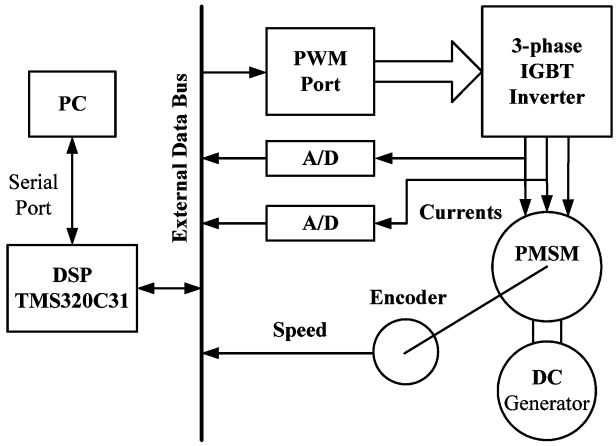

Fig. 5. Configuration of DSP-based experimental setup.

of the PI speed controller are: $K_p = 0.035, K_i = 0.35$, while the gains of the PI current controllers: $K_p = 40, K_i = 600$. The learning gains are: $\Phi = 0.4, \Gamma = 0.02$. Forgetting factor $\alpha = 0.05$. Parameter N is chosen as 12, since only harmonics of order lower than or equal to 12 are considered in our study.

The photograph of a PMSM coupled with a dc generator used as loading mechanism is shown in Fig. 4, whereas Fig. 5 shows the configuration of the experimental setup. Although there is a torque transducer coupled along the motor shaft, it is not actually used in our proposed schemes, since we only need speed information instead of torque signal. The motor parameters are listed in Table I. The proposed control scheme is realized in the DSP-based drive setup using the floating-point 60-MHz DSP TMS320C31. The proposed algorithm is implemented using C-program. Currents of two phases are measured using Hall-effect devices and then converted into digital value using 16-bit A/D converters.

TABLE I
MOTOR PARAMETERS

Rated power	1.64 kW
Rated speed	2000 rpm
Stator resistance	2.125 Ω
Stator inductance	11.6 mH
Magnet flux	0.387 Wb
Number of poles	6
Inertia	0.03 kg·m^2

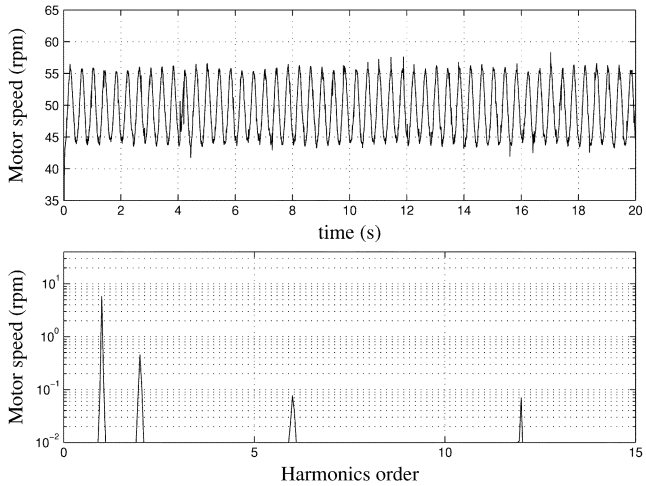

Fig. 6. Speed response without ILC compensation ($\omega_m = 50$ r/min, $T_l = 0.0$ Nm).

The performance evaluation of the proposed ILC control in suppressing torque ripples is presented in the following section.

VI. EXPERIMENTAL RESULTS AND DISCUSSIONS

A. Experimental Results

To verify the effectiveness of the proposed ILC schemes, experiments are carried out using the DSP-based PMSM drive system described in the previous section. The experiments were conducted under different operating conditions, with speeds ranging from 0.005 p.u. (10 r/min) to 0.05 p.u. (100 r/min) and load torques from 0.0 p.u. to 0.795 p.u. (6.20 Nm). The performance criterion to evaluate the effectiveness of the proposed scheme for speed ripple minimization is the speed ripple factor (SRF). It is defined as the ratio of the peak-to-peak speed ripple to the rated speed of the PMSM (29)

$$\text{SRF} = \frac{\omega_{pk-pk}}{\omega_{\text{rated}}} \times 100\%. \tag{29}$$

The SRF of the PMSM drive using the conventional PI speed controller alone is first determined. Subsequently, the proposed ILC controller which generates compensation current is applied in parallel and the corresponding SRF is re-evaluated. Figs. 6–11 each shows the speed response in time domain (the upper plot) and in the corresponding frequency spectrum (the lower plot). For the purpose of clearness, we pick up only the 1st, 2nd, 6th, and 12th harmonics which are of interest and show them in the frequency spectrum. Fig. 6 shows the speed waveform when the motor runs at 0.025 p.u. (50 r/min) under

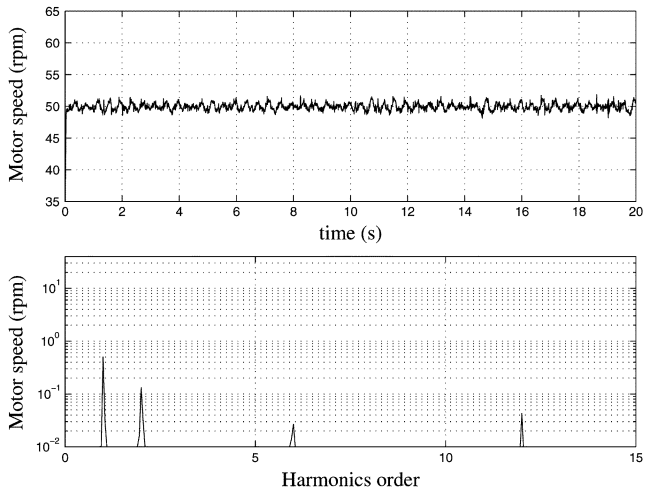

Fig. 7. Speed response with time-domain ILC compensation ($\omega_m = 50$ r/min, $T_l = 0.0$ Nm).

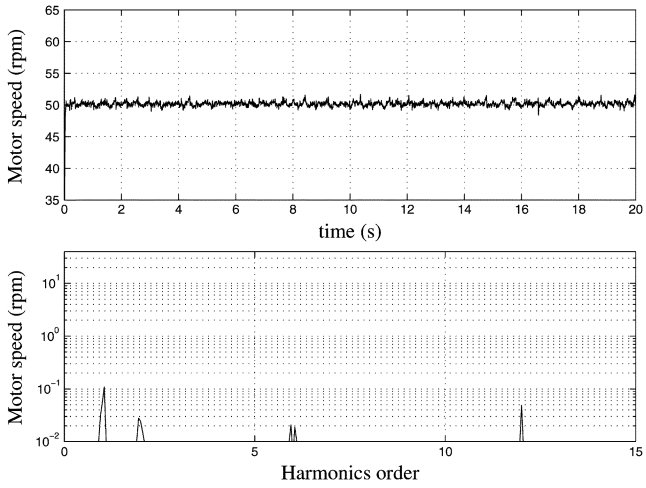

Fig. 8. Speed response with frequency-domain ILC compensation ($\omega_m = 50$ r/min, $T_l = 0.0$ Nm).

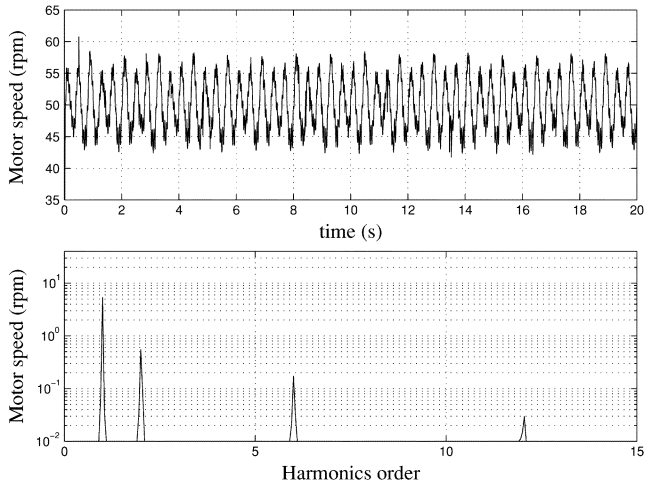

Fig. 9. Speed response without ILC compensation ($\omega_m = 50$ r/min, $T_l = 6.20$ Nm).

no external load torque and without ILC compensation. In this figure, a large speed oscillation can be observed with the corresponding $\mathrm{SRF} = 0.65\%$. Figs. 7 and 8 present the speed

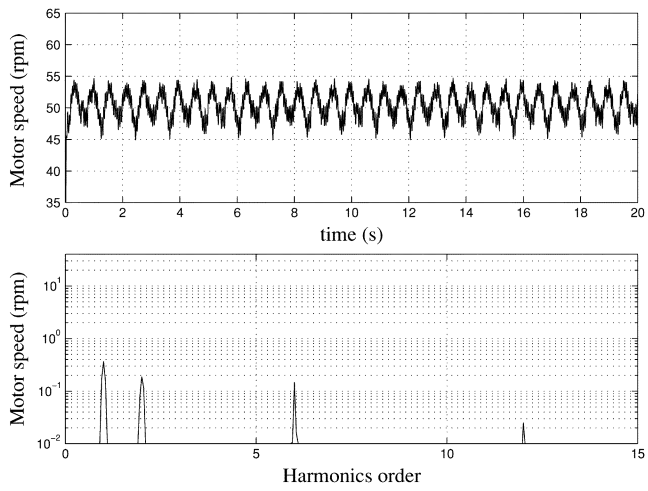

Fig. 10. Speed response with time-domain ILC compensation ($\omega_m = 50$ r/min, $T_l = 6.20$ Nm).

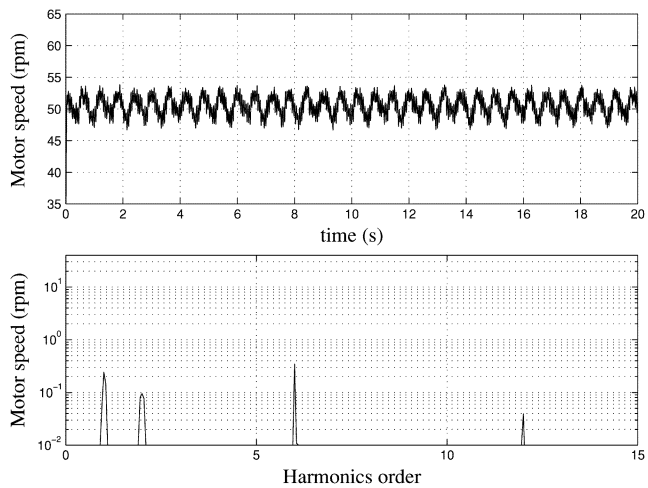

Fig. 11. Speed response with frequency-domain ILC compensation ($\omega_m = 50$ r/min, $T_l = 6.20$ Nm).

waveforms under the same working condition with ILC compensation schemes implemented in the time domain and frequency domain, respectively. We can see that speed ripple harmonics are reduced with the $\mathrm{SRF} = 0.15\%$ after applying the time-domain ILC scheme. Further reduction is possible by using the frequency domain learning method with the SRF reduced to 0.10%, comparing the 1st, 2nd, and 6th harmonics in Fig. 7 with those in Fig. 8.

Figs. 9–11 are arranged in the same sequence, and the operating conditions for these figures are $\omega_m = 0.025$ p.u. (50 r/min), $T_i = 0.795$ p.u. (6.20 Nm). It can be seen again that both the proposed schemes are able to compensate for the 1st and 2nd harmonic components to a greater extent. However, the reduction in the 6th and 12th components is not so considerable as the case without load. This is because when motor operates under heavy loads, the dc generator is coupled and excited for loading purpose, and the resultant torque pulsations induced from the load side that mainly consist of noninteger harmonics become greater. They are reflected back in speed ripples, which cannot be compensated by the ILC schemes due to their noninteger multiples of the fundamental frequency nature.

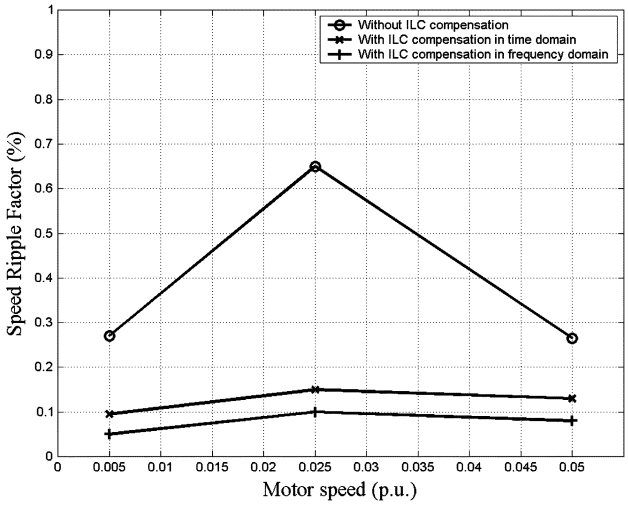

Fig. 12. SRFs of different speeds under no external load without and with ILC compensation.

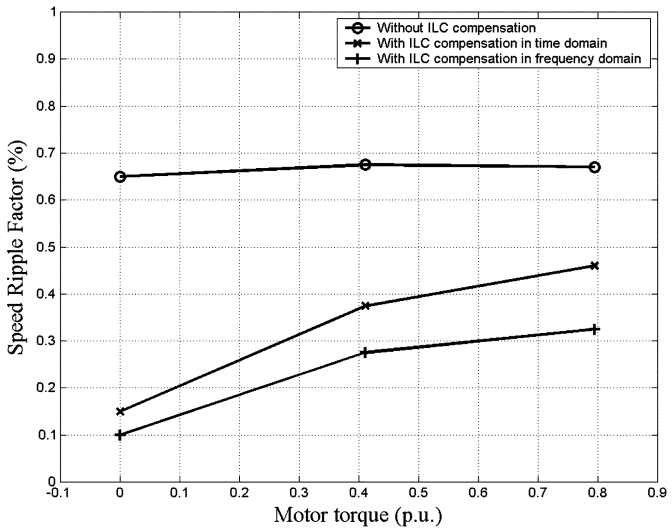

Fig. 13. SRFs of different load torques with speed at 50 r/min without and with ILC compensation.

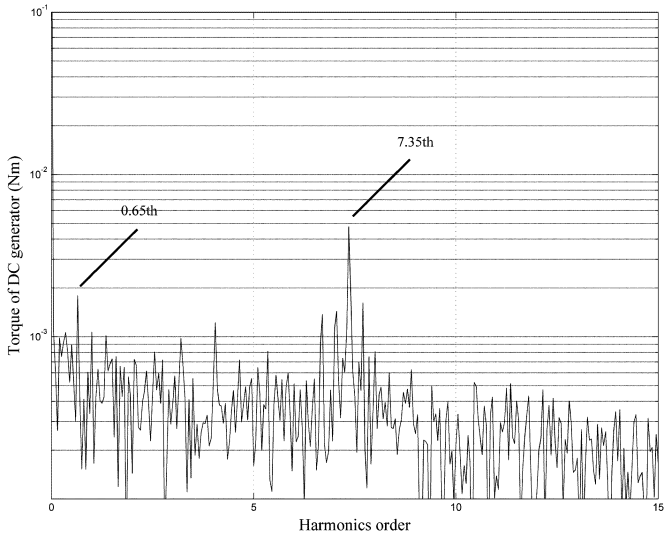

Fig. 14. Frequency spectrum of torque pulsations induced by the dc generator.

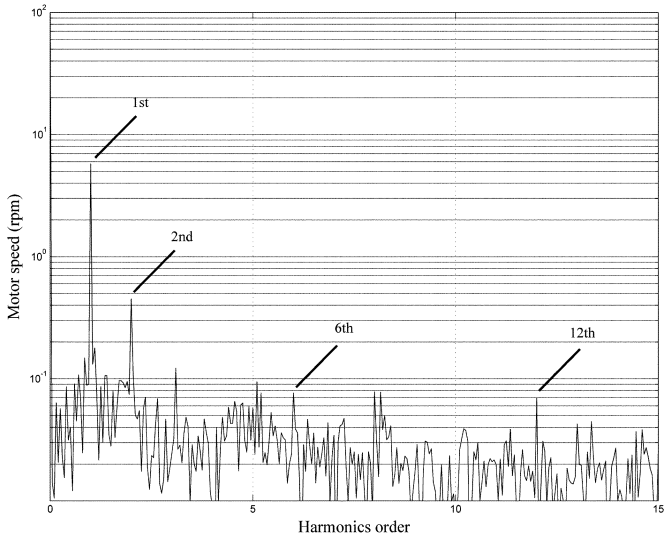

Fig. 15. Frequency spectrum of speed response without ILC compensation ($\omega_m = 50$ r/min, $T_l = 0.0$ Nm).

The detailed SRFs under different working conditions are shown in Figs. 12 and 13. The former gives the SRFs when PMSM operates at different speeds: 0.005 p.u. (10 r/min), 0.025 p.u. (50 r/min) and 0.05 p.u. (100 r/min), under no external load without and with both ILC compensation schemes. The latter shows the SRFs when PMSM operates at 0.025 p.u. (50 r/min) under different load torques: 0.0 p.u., 0.410 p.u. (3.2 Nm), and 0.795 p.u. (6.2 Nm), without and with both ILC compensation schemes. According to the results, the effectiveness of the proposed ILC schemes is verified in suppressing speed ripples under various steady-state operating conditions. As in Fig. 12, it can be seen that the SRF is relatively high when motor runs at 50 r/min, since at this speed the peak-to-peak speed ripple reaches maximum and so does SRF [12].

From the experimental results presented, apparently, it can be seen that the ILC scheme implemented in frequency domain by means of Fouier series expansion is better than that implemented in time domain. This is because the time-domain learning cannot eliminate errors totally due to the introduction of forgetting factor [14]. However, there is still a disadvantage in the frequency-domain learning when it faces the problem caused by the existence of those noninteger harmonics induced from the load side, which will be explained in the following subsection.

B. Torque Pulsations Induced by the Load

It is necessary to distinguish those torque ripples caused by loading mechanism from the ones induced by the PMSM, which are of our interest. For this purpose, we decouple the PMSM from the dc machine, which is originally used as the load, excite the dc machine to work in the motoring mode at 50 r/min, and observe the torque signal by using a torque transducer. Fig. 14 shows the frequency spectrum of the resultant torque pulsations induced by the dc machine alone. It can be seen that some noninteger harmonics are present in the torque waveforms, among which the 0.65th and 7.35th harmonics are dominant. In addition, energy distributed around the 7th and 8th harmonics are quite apparent. Figs. 15 and 16 show the frequency spectrum of speed response without ILC compensation under the light load

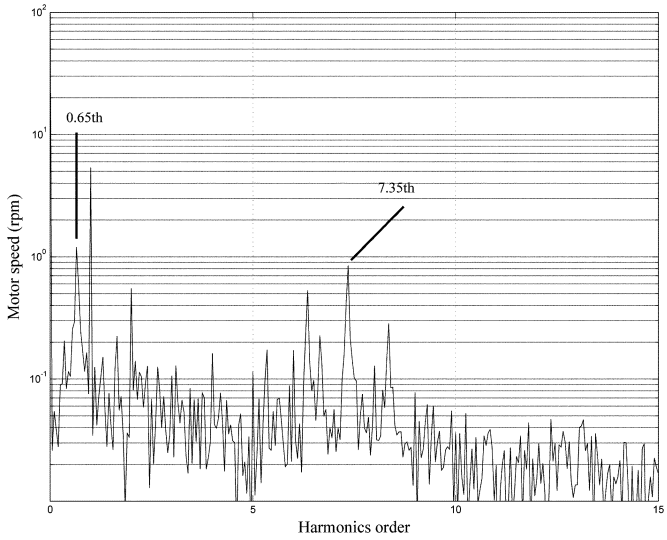

Fig. 16. Frequency spectrum of speed response without ILC compensation ($\omega_m = 50$ r/min, $T_l = 6.20$ Nm).

and heavy load, respectively. In Figs. 15, we can observe that the integer multiple harmonics are the most dominant components, while in Fig. 16, noninteger harmonics, the 0.65th and 7.35th components become invincible. In fact, these components are the same dominant harmonics which appear in Fig. 14, since they are induced by the nonideal load mechanism when the dc machinery is excited for heavy load purposes.

It should be noted that the ILC control schemes presented in this paper are supposed to reduce speed harmonics, which are integer multiples of fundamental frequency. This is because ILC is designed in face of removing periodic disturbance in the input, and it has no effect on nonperiodic disturbance. In our case, speed ripples caused by torque oscillations are periodic in nature, and most of these speed ripples share the same period. Thus, we define this time period as the basic period in the ILC schemes implementation so as to remove most of these speed ripples. However, those noninteger harmonics induced from the load side are ripples that do not share that basic time period with others, which makes them impossible to be eliminated by using ILC. To solve this problem, we can multiply the basic time period such that those noninteger harmonics become "integers" in corresponding with the new period. However, this will prolong the converging time of learning process, and such method is noneffective in case of pseudoharmonics, because it is impossible to find its time period.

This nonideal loading mechanism, namely the appearance of noninteger torque harmonics further degrades the performance of the proposed controllers, particularly the frequency-domain learning method. Although a Fourier-based learning mechanism is capable of further reduction of speed ripples, it also induces a distorted approximation of these noninteger harmonics. Such distortion is caused by the mismatch between the time period of Fourier transformation and those of noninteger harmonics. As a result, this incorrect information further induces the error accumulation during the learning process, which makes the ILC scheme implemented in frequency domain less desirable when facing the nonideal situation of load mechanism. This also explains why the 6th harmonics has been increased a little in Fig. 11, since the distortion of error information affects the local bandwidth and generates locally wrong control signals to compensate for the speed ripples.

VII. Conclusion

Two periodic speed ripple minimization schemes, which are implemented in time domain and frequency domain respectively, using iterative learning control are presented in this paper. Learning control is intuitively an excellent selection for the speed ripples minimization scheme because of the periodic nature of torque and hence speed ripples. Moreover, the scheme is simple to implement, can be added to any existing controller and does not require accurate knowledge of the motor parameters. The learning control scheme implemented in time domain guarantees minimization of the speed ripples to a certain extent, but further improvement is limited by the introduction of the forgetting factor in the algorithm. Therefore, a learning method in the frequency domain by means of Fourier series expansion is designed to further suppress the speed ripples. However, such method has a disadvantage when facing the noninteger or pseudo harmonics present in the nonideal loading mechanism. Experimental investigations were conducted on an integrated DSP-based PMSM platform. Both schemes are verified effective in minimizing periodic speed ripples caused by PMSM drive system and nonsymmetrical construction of the motor.

References

[1] T. M. Jahns and W. L. Soong, "Pulsating torque minimization techniques for permanent magnet ac drives—A review," *IEEE Trans. Ind. Electron.*, vol. 43, no. 2, pp. 321–330, Apr. 1996.

[2] C. Studer, A. Keyhani, T. Sebastian, and S. K. Murthy, "Study of cogging torque in permanent magnet machines," in *Proc. IEEE 32nd Ind. Appl. Society (IAS) Annu. Meeting*, vol. 1, New Orleans, LA, Oct. 1997, pp. 42–49.

[3] J. Y. Hung and Z. Ding, "Design of currents to reduce torque ripple in brushless permanent magnet motors," *Proc. Inst. Elect. Eng. B*, vol. 140, no. 4, pp. 260–266, 1993.

[4] D. C. Hanselman, "Minimum torque ripple, maximum efficiency excitation of brushless permanent magnet motors," *IEEE Trans. Ind. Electron.*, vol. 41, no. 3, pp. 292–300, Jun. 1994.

[5] J. Holtz and L. Springob, "Identification and compensation of torque ripple in high-precision permanent magnet motor drives (invited paper)," *IEEE Trans. Ind. Electron.*, vol. 43, no. 2, pp. 309–320, Apr. 1996.

[6] V. Petrović, R. Ortega, A. M. Stanković, and G. Tadmor, "Design and implementation of an adaptive controller for torque ripple minimization in PM synchronous motors," *IEEE Trans. Power Electron.*, vol. 15, no. 5, pp. 871–880, Sep. 2000.

[7] T. S. Low, T. H. Lee, K. J. Tseng, and K. S. Lock, "Servo performance of a BLDC drive with instantaneous torque control," *IEEE Trans. Ind. Appl.*, vol. 28, no. 2, pp. 455–462, Mar./Apr. 1992.

[8] N. Matsui, T. Makino, and H. Satoh, "Autocompensation of torque ripple of direct drive motor by torque observer," *IEEE Trans. Ind. Appl.*, vol. 29, no. 1, pp. 187–194, Jan./Feb. 1993.

[9] S. K. Chung, H. S. Kim, C. G. Kim, and M.-J. Youn, "A new instantaneous torque control of PM synchronous motor for high-performance direct-drive applications," *IEEE Trans. Power Electron.*, vol. 13, no. 3, pp. 388–400, May 1998.

[10] F. Colamartino, C. Marchand, and A. Razek, "Torque ripple minimization in permanent magnet synchronous servodrive," *IEEE Trans. Energy Conversion*, vol. 14, no. 3, pp. 616–621, Sep. 1999.

[11] P. C. Krause, *Analysis of Electric Machinery*. New York: McGraw-Hill, 1987.

[12] D. W. Chung and S. K. Sul, "Analysis and compensation of current measurement error in vector-controlled ac motor drives," *IEEE Trans. Ind. Appl.*, vol. 34, no. 2, pp. 340–345, Mar./Apr. 1998.

[13] Z. Bien and J.-X. Xu, *Iterative Learning Control—Analysis, Design, Integration, and Applications*. Boston, MA: Kluwer, 1998.

[14] S. Arimoto, T. Naniwa, and H. Suzuki, "Robustness of P-type learning control with a forgetting factor for robotic motions," in *Proc. 1990 IEEE Decision and Control Conf.*, vol. 5, Dec. 5–7, pp. 2640–2645.
[15] S. Boming, "On Iterative Learning Control," M.Eng. thesis, National Univ. of Singapore, 1997.
[16] J.-X. Xu and W.-J. Cao, "Learning variable structure control approaches for repeatable tracking control tasks," *Automatica*, vol. 37, no. 7, pp. 997–1006, Jul. 2001.

Weizhe Qian was born in Shanghai, China, in 1978. She received the B.Eng. degree in electric power engineering from Shanghai Jiao Tong University in 2001. She is currently pursuing the Master's degree in the Department of Electrical and Computer Engineering, National University of Singapore.

S. K. Panda (SM'03) received the B.Eng. degree from South Gujarat University, India, in 1983, the M.Tech. degree from IT, BHU, India, in 1987, and the Ph.D. degree from the University of Cambridge, Cambridge, U.K., in 1991.

Since 1992, he has been a Faculty Member in the Department of Electrical and Computer Engineering, National University of Singapore, and currently serves as an Associate Professor. His research interests include control of electrical drives and power-electronic-based systems.

Dr. Panda has served as the Technical Program Chairman of the IEEE PEDS'97 Conference and is the Organizing Chairman of IEEE PEDS'03 Conference. He received the IEEE Third Millennium Medal.

J. X. Xu (SM'98) was born in Beijing, China, in 1957. He received the Bachelor's degree from Zhejiang University, China, in 1982 and the Master's and Ph.D. degrees from the University of Tokyo, Tokyo, Japan, in 1986 and 1989, respectively, all in electrical engineering.

He was with Hitachi Research Laboratory, Japan, and Ohio State University, Columbus, as a Visiting Scholar, during 1989–1991. In 1991, he joined the National University of Singapore, where he is currently an Associate Professor in the Department of Electrical Engineering. His research interests lie in the fields of learning control, variable structure control, fuzzy logic control, and discontinuous signal processing.